Chinese Science Bulletin

Response of the magnetic field and plasmas at the geosynchronous orbit to interplanetary shock

YUE Chao, ZONG QiuGang† & WANG YongFu

Institute of Space Physics and Applied Technology, Peking University, Beijing 100871, China

Interplanetary shock can greatly disturb the Earth's magnetosphere and ionosphere, causing the temporal and spatial changes of the magnetic field and plasmas at the geosynchronous orbit. In this paper, we use the magnetic field data of GOES satellites from 1997 to 2007 and the plasma data of MPA on the LANL satellites from 1997 to 2004 to study the properties of magnetic field and plasma (0.03−45 keV) at the geosynchronous orbit (6.6 R_E) within 3 hours before and after the arrival of shock front at the geosynchronous orbit through both case study and superposed epoch analysis. It is found that following the arrival of shock front at the geosynchronous orbit, the magnetic field magnitude, as well as GSM B_Z component increases significantly on the dayside (8−16 LT), while the B_Y component has almost no change before and after shock impacts. In response to the interplanetary shock, the proton becomes much denser with a peak number density of 1.2 cm^{-3}, compared to the typical number density of 0.7 cm^{-3}. The proton temperature increases sharply, predominantly on the dusk and night side. The electron, density increases dramatically on the night side with a peak number density of 2.0 cm^{-3}. The inferred ionospheric O^+ density after the interplanetary shock impact reaches the maximum value of 1.2 cm^{-3} on the dusk side and exhibits the clear dawn-dusk asymmetry. The peak of the anisotropy of proton's temperature is located at the noon sector, and the anisotropy decreases towards the dawn and dusk side. The minimum of temperature anisotropy is on the night side. It is suggested that the electromagnetic ion cyclotron (EMIC) wave and whistler wave can be stimulated by the proton and electron temperature anisotropy respectively. The computed electromagnetic ion cyclotron wave (EMIC) intense on the day side (8−16 LT) with a frequency value of 0.8 Hz, and the wave intensity decreases towards the dawn and dusk side, the minimum value can be found on the night side. The computed electron whistler wave locates on the day side (8−16 LT) with a value of 2 kHz.

interplanetary shock, geosynchronous orbit, superposed epoch analysis, electromagnetic ion cyclotron wave, whistler wave

The geosynchronous orbit normally connects the inner boundary of the plasma sheet near the tail region and outer boundary of the inner magnetosphere (including the plasmasphere) and is an ideal location to study the particle acceleration and plasma transport mechanisms from the magnetotail into the inner magnetosphere. Many satellites located at the geosynchronous orbit can be used to monitor the temporal and spatial changes of plasma and magnetic field, such as NOAA's series of GOES satellites and the LANL satellites. Until now, many researchers have done a lot of work about the geosynchronous orbit, such as the response of the magnetic field at the geosynchronous orbit to the solar wind GOES 5, and GOES 6 spacecraft. They found that, for the magnetic field variations observed by GOES 2, quiet

Received July 27, 2009; accepted August 26, 2009
doi: 10.1007/s11434-009-0649-6
† Corresponding author (email: qgzong@pku.edu.cn)
Supported by the National Natural Science Foundation of China (Grant No. 40831061)

Citation: Yue C, Zong Q G, Wang Y F. Response of the magnetic field and plasmas at the geosynchronous orbit to interplanetary shock. Chinese Sci Bull, 2009, 54: 4241−4252, doi: 10.1007/s11434-009-0649-6

dynamic pressure changes. Rufenach et al.[1] analyzed conditions (AE<120 nT and $|D_{st}|$<20 nT), the average value of the magnetic field measured by the GOES satellites generally increases when the hourly-averaged solar wind dynamic pressure increases. Wang et al.[2] statistically surveyed the responses of geosynchronous magnetic fields to the solar wind dynamic pressure pulses in geomagnetic quiet times with D_{st} > –50 nT and used a global solar wind-magnetosphere-ionosphere MHD code to reproduce the main observation characteristics. Patel and Coleman[3] reported that sudden impulses including 13 events in 1967 at the geosynchronous orbit had smaller amplitude on the night side than those on the day side. Lee and Lyons[4] analyzed 35 sudden impulses events during 1997—2001 and concluded that solar wind pressure enhancements generally lead to a magnetospheric compression at all time sectors with few exceptions on the night side. Borodkova et al.[5] found that 147 out of 261 changes of the solar wind dynamic pressure (positive and negative; 1996—1998) were associated with corresponding variations of the magnetospheric field (GSM B_Z component). They also remarked that all the events without an explicit response were located either before 7:30 LT or after 16:30 LT. Lee et al.[6] examined the geosynchronous energetic particles' response to solar wind dynamic pressure enhancements and suggested that, during northward IMF conditions, simple compression effects were observed on the day side and night side, whereas during southward IMF conditions, a dipolarization of the geomagnetic field associated with current wedge formation was observed on the night side and a simple compression was detected on the day side. Analysis of sudden impulses (SI) including 55 events during 2000—2004 at the geosynchronous orbit made by Villante and Piersanti[7] confirmed a general dependence of the SI amplitude on the variation of the square root of the solar wind dynamic pressure, together with an explicit LT dependence, with greater responses at satellites located closer to noon meridian.

The interplanetary shock is an abrupt boundary which formed at the front of a plasma cloud (e.g. Coronal Mass Ejection, CME). At the upstream the propagating speed is supersonic and at the downstream the propagating speed is subsonic. Recently, Wang et al.[8] performed a statistical survey of geospace magnetic field responses, including the geosynchronous magnetic field and the sudden impulses on the ground, to interplanetary shocks (IP shocks) between 1998 and 2005. They concluded that the magnitude of the geosynchronous magnetic field (dBz) responses to IP shocks depends strongly on local time, which peaks near the noon meridian. For a moderately compressed magnetosphere, the amplitude of the geosynchronous response dBz could be determined by the average value of the background local magnetic field and the dBz at the geosynchronous orbit near local noon was correlated to the amplitude of sudden impulses (dSYM-H) on the ground are highly.

Recently, many studies have been addressed on the mechanism of energy particles injected into the geosynchronous orbit. For example, Borovsky et al.[9] analyzed the transport of plasma sheet material from the magnetotail to the geosynchronous orbit and found that earthward transport is stronger when the solar wind velocity is relative lower. For the location of particles injected into the geosynchronous orbit, Elphic et al.[10] showed that the plasmaspheric density observed at the geosynchronous orbit is peaked near 14 LT due to magnetospheric compression and the increasing of the convection electric field. This is greatly skewed from the average plasmaspheric distribution at the geosynchronous orbit which peaks close to 18 LT. Using a full year of data of substorm times from spacecraft at the geosynchronous orbit, Birn et al.[11] examined the behavior of the thermal plasma (30 eV < E < 40 keV) in the plasma sheet by superposed epoch analysis. They found that the ion injecting location is about 3 hours prior to local midnight, while the electron injecting location is about 2 hours after midnight. For the magnetosphere response to the ICME shock, Dandouras et al.[12] showed the observations by Cluster and Double Star during the 2005 and 2006 extreme solar events. They found that solar wind velocities up to ~900 $km \cdot s^{-1}$ during the ICME shock arrival, accompanied by a sudden increase in the density by a factor of ~5. In the magnetosheath ion density reached the maximum value of 130 cm^{-3} and the plasma flow velocity is much higher than the typical solar wind velocity. These resulted in unusual dayside magnetosphere compression. The ring current enhanced following several successive injections of energetic particles from the magnetotail.

On the base of superposed epoch analysis method, many important results have been obtained. Borovsky and Denton[13] have studied the relativistic electron dropouts and recovery mechanism at the geosyn-

chronous orbit during high-speed-stream-driven storms. They found that the onset of dropout occurs after the passage of the IMF sector reversal prior to the passage of the corotating interaction region (CIR) stream interface, and the recovery from dropout commences during the passage of the compressed fast wind. Denton et al.[14] performed a superposed epoch analysis of 283 geomagnetic storms to present a comprehensive study of plasma (0.001－45 keV) properties at the geosynchronous orbit during 1990－2001. They found that the electron and proton densities in the dawn region are the highest for the periods of largest convection and ring current strength. They also outline a method to estimate the composition of the plasma sheet from MPA measurements and calculate the O^+ and H^+ density variations with solar cycle as a function of *K*p and the local time. They show that the O^+ and H^+ plasma sheet densities increase with increasing solar activity, as does the O^+/H^+ density ratio. Denton and Borovsky[15] performed a superposed epoch analysis to reveal the density, temperature and flow velocity behavior of the hot ion plasma (0.1－45 keV), the hot electron plasma (0.03－45 keV) and the cold ion plasma (1－100 eV) at the geosynchronous orbit following the arrival of high speed solar wind streams at the dayside magnetopause.

On the other hand, we know that ions with energies of a few tens of keV, are able to stimulate the EMIC wave in frequency below $\omega/\Omega_i < A_i/(1+A_i)$, where $A_i = T_\perp/T_\parallel - 1$ is the temperature anisotropy, Ω_i is the ion gyrofrequency of any ion species and $T_\perp$ and $T_\parallel$ are the ion perpendicular and parallel temperature with regard to the magnetic field direction respectively[16]. EMIC waves in the Pc1 frequency range (0.2－5 Hz) provide an important mechanism to transfer energy between different particle populations and to transport energy within the magnetosphere[17]. Kennel and Petschek[16] and Cornwall et al.[18] proved that large-amplitude EMIC waves can cause rapid pitch angle scattering and precipitation and thus contribute to the loss of ring current ions. Thorne and Horne[19] and Cornwall et al.[20] found that the EMIC waves can heat thermal electrons via electron Landau damping and thus contribute to the source of an electron heat flux into the ionosphere, which is responsible for the generation of stable auroral red arcs. Bossen et al.[21] reported that outside the plasmapause, near the geostationary orbit, strong EMIC waves (with wave amplitude of 1－7 nT) were often detected in the afternoon sector with frequencies between 0.1 and 0.2 Ω_{H^+}. Since natural space plasmas are collisionless plasmas, the energy particles can generally be well modeled by a generalized Lorentzian (kappa) distribution[22,23]. The studies taken by Xiao et al.[24–26] have shown that the instability threshold condition for the EMIC waves and the whistler mode waves for the kappa distribution is different from those for the regular bi-Maxwellian distribution. The instability threshold condition for the kappa distribution generally decreases as the spectral index κ increases and tends to the lowest limiting values of the bi-Maxwellian as $\kappa \to \infty$. The instability threshold condition for the whistler mode waves in the higher-density (or a weakly magnetized) region is generally lower than that in the lower-density (or a strongly magnetized) region.

As mentioned previously, most studies focused on the magnetic field or plasmas at geosynchronous orbit during the increasing of solar wind dynamic pressure, magnetic storms or substorms. Few statistical analyses have been done with respect to interplanetary shock impact of the plasma behavior at the geosynchronous orbit. In this paper, we use both case study and the superposed epoch analysis method to study the properties of magnetic field and plasma (0.03－45 keV) at the geosynchronous orbit within 3 hours before and after the arrival of shock front at the geosynchronous orbit, using the data of the magnetic field from GOES satellites from 1997 to 2007 and the plasma from MPA on the LANL satellites from 1997 to 2004.

1 Data sources and analysis methods

In this paper, we have studied a total of 144 shock events (we take the published shock events on the website of http://umtof.umd.edu/pm/Figs.html as reference). The arriving time of the interplanetary shock is based on the observations of ACE or WIND satellite, the onset of the arrival of shock front at the geosynchronous orbit can be referred from the properties of proton and electron fluxes which is plotted on the website of http://leadbelly.lanl.gov/lanl_ep_data/cgi-bin/ep_plot_choose_3.cgi. We use 1-min resolution of

GOES-8, GOES-9, GOES-10, GOES-11 and GOES-12 geosynchronous magnetic field data[27] which cover an entire 11 year solar cycle from 1997 to 2007. There are only 135 events in which magnetic field data are available and the details are shown in Table 1. The plasma data are got from Magnetospheric Plasma Analyzer (MPA)[28, 29] on the LANL satellites data set at the geosynchronous orbit and cover from 1997 to 2004. In the current study we use the density, temperature and the temperature anisotropy for the hot electrons (HE) in the energy range from 0.03 to 45 keV, the hot protons (HP) in the energy range from 0.1 to 45 keV. There are only 90 events in which the plasma data are available and the details are shown in Table 1. The data are extracted from all available LANL satellites and GOES satellites during each of the 144 shock events and rearranged on the base of the epoch of the arrival of shock front at the geosynchronous orbit. The magnetic field data are binned according to epoch time (1 min resolution) and local time (2 h resolution) from 3 hour prior to the onset to 3 hour following the shock arrival. The MPA Data are binned according to epoch time (5 min resolution) and local time (2 h resolution) from 3 hour prior to the onset to 3 hour following the shock arrival. The resulting data series reflect the magnetic field and plasmas properties with the zero time epoch being the interplanetary shock arrival time.

Table 1 The distribution of the 144 shock events

Year	Number of shock events	Number of available events about magnetic field	Number of available events about plasma
1997	7	7	7
1998	8	7	6
1999	12	11	4
2000	19	19	14
2001	28	27	16
2002	22	22	12
2003	21	21	21
2004	12	12	10
2005	8	3	
2006	4	4	
2007	3	3	

2 Case study

The July 22, 2004 event is one of the best examples in our data set to illustrate the events selected in this study. Figure 1 shows the solar wind parameters observed by ACE satellite at the L1 point. At 09:53 UT, the proton number density increased from 3 cm^{-3} to 15 cm^{-3}, the radial temperature, the total magnetic field, the solar wind speed and solar wind dynamic pressure (from 0.8 to 6 nPa) are significantly enhanced. The shock front reached the geosynchronous orbit at 10:34 UT. The plots about the magnetic field and plasma parameters are shown in Figures 2—4.

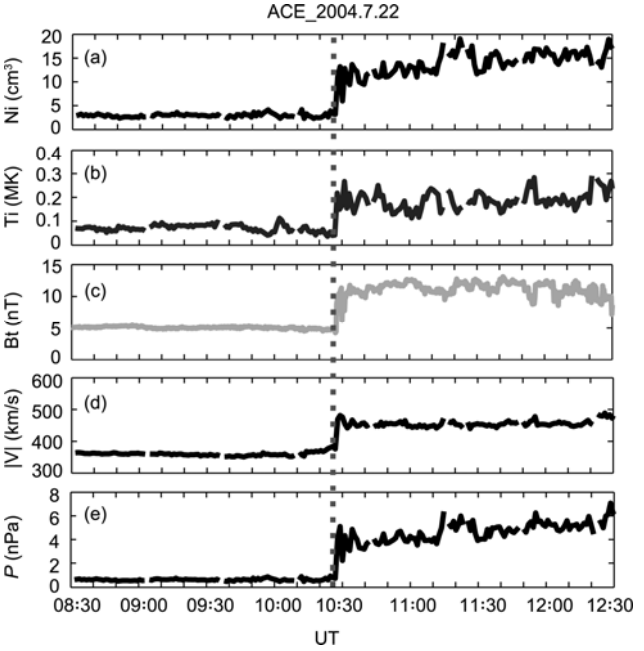

Figure 1 Interplanetary magnetic field and solar wind parameters observed by ACE satellite. (a) The proton number density; (b) the radial temperature; (c) the total magnetic field; (d) the solar wind speed; (e) solar wind dynamic pressure. The dashed line marks the arrival of interplanetary shocks.

Figure 2 shows that the magnetic field at the geosynchronous orbit had a sudden increase when the shock front reached the geosynchronous orbit. B_X linearly is decreased prior to the onset，and suddenly increased following the onset, then decreased with fluctuations. B_Y and B_Z component and the magnetic field magnitude increase steadily prior to the onset. When the shock front arrived the geosynchronous orbit, B_Y and B_Z components, as well as the total magnetic field increase by around 10 nT in short time. Following the onset, B_Z component and the total magnetic field increased smoothly, the maximum of total magnetic field is close to 140 nT.

Figure 3 shows the results of July 22, 2004 event for proton density, the perpendicular and parallel tempera-

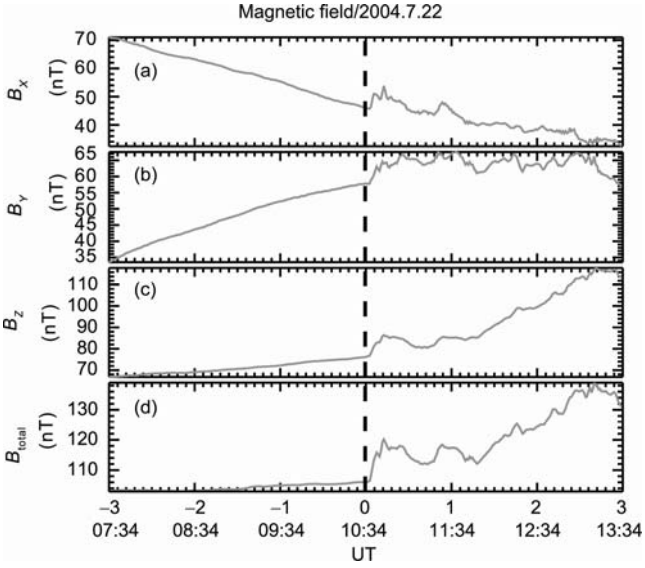

Figure 2 The magnetic field of July 22, 2004 event observed by GOES 12 at the geosynchronous orbit. (a) GSM B_X component; (b) GSM B_Y component; (c) GSM B_Z component; (d) the magnetic field magnitude. The dashed line marks the shock arrival at the geosynchronous orbit.

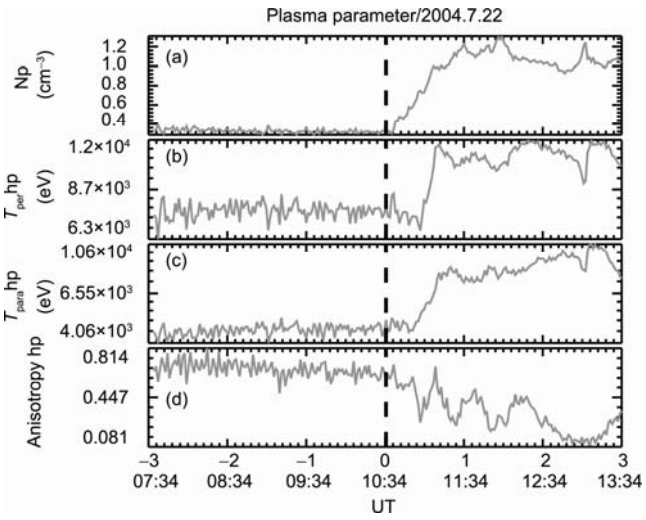

Figure 3 Hot proton (HP) measurements at the event of July 22, 2004. (a) HP number density; (b) HP perpendicular temperature; (c) HP parallel temperature; (d) HP temperature anisotropy. The dashed line marks the shock arrival at the geosynchronous orbit.

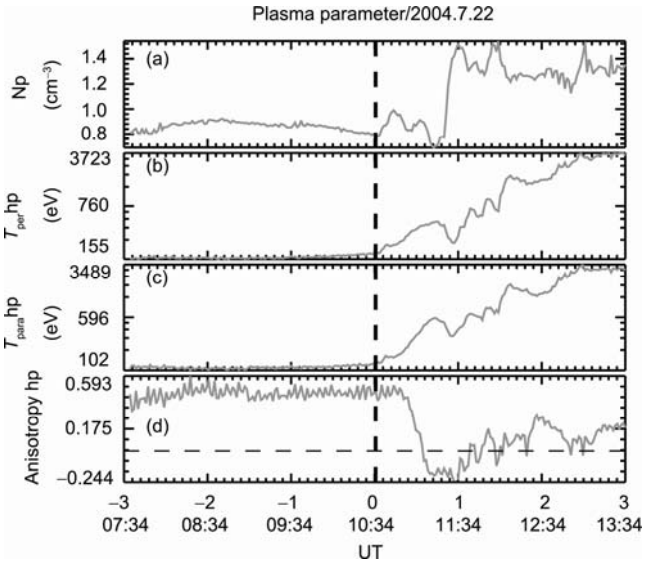

Figure 4 Hot electron (HE) measurements at the event of July 22, 2004. (a) HE number density; (b) HE perpendicular temperature; (c) HE parallel temperature; (d) HE temperature anisotropy. The dashed line marks the shock arrival at the geosynchronous orbit.

tures and temperature anisotropy at the geosynchronous orbit. Prior to the arrival of shock front at geosynchronous orbit onset, proton density, the perpendicular and parallel temperatures and temperature anisotropy were stable, accompanied with small amplitude fluctuations. Following the onset, the ion density increased rapidly from 0.4 cm^{-3} to 1.3 cm^{-3} in 40 min. The perpendicular and parallel temperatures had a lagged response with respect to the shock arrival. The lag effect may be somehow related to the location of GOES satellite. As can be seen from Figure 3, 20 min after the shock arrival at the geosynchronous orbit, the proton perpendicular and parallel temperatures increased by about 6000 eV in short time, then became stable and accompanied with small amplitude fluctuations. Proton temperature was stable prior to the onset and fluctuated fiercely after the onset. For electron, as shown in Figure 4, electron density, temperature and temperature anisotropy almost had no change prior to the arrival of shock front. Following the onset, the electron density, the perpendicular and parallel temperatures increased dramatically, but the temperature anisotropy sharply decreased, from 0.6 down to – 0.2 in 10 min.

It can be seen from the July 22, 2004 case that the interplanetary shock has short-term impact on the magnetic field and plasma at the geosynchronous orbit, the corresponding time scale is about 2 hours. However, the temporal and spatial variation of the magnetic field and plasma cannot be distinguished from case study. Therefore, we will use the superposed epoch analysis to study the temporal and spatial responses of the magnetic field and plasma at the geosynchronous orbit to the interplanetary shock in the following section.

3 Response of the magnetic field and plasmas in the geosynchronous orbit to the interplanetary shock

3.1 Interplanetary shock induced magnetic field variations at the geosynchronous orbit

Figure 5 shows the results of superposed epoch analysis for the magnetic field magnitude for all available shock events. The magnetic field magnitude enhanced abruptly on the day side following the zero epoch, from 120 nT to 160 nT. This result is consistent with the study of Wang et al.[8]. It is because that the magnetosphere is compressed from the dayside magnetopause by the shock, making the magnetic field magnitude enhanced.

Figure 6 shows the results of superposed epoch analysis for magnetic field in GSM for all available events. Prior to the zero epoch, the local distribution of B_X and B_Y components are contrary to the distribution of B_Z component. B_X is stronger in the evening sector, B_Y is stronger at the local time location of 2－8 LT, while B_Z is stronger on the day side (8－16 LT) and gradually decreases towards the night side. Following zero epoch, B_X increased only on the day side (8－16 LT) and almost has no change on the night side before and after the shock front arrival. B_Y almost has no change before and after the shock front arrival. B_Z component increases on the day side with the maximum of 160 nT while decreases on the night side.

3.2 Density and temperature of proton response at the geosynchronous orbit

Figure 7 shows the result of superposed epoch analysis for the hot proton (0.1－45 keV) number density for all available events. Prior to the zero epoch, the proton has typical density distribution which is higher on the night side. Following the zero epoch, the proton density increases at all local time. The proton density decreases in the noon sector and significantly enhances in other sectors half an hour after the shock front arrival. Two hours after the zero epoch, the proton density reaches the maximum value of 1.2 cm^{-3} on the night side.

Figure 8 shows the results of superposed epoch analysis for the hot proton (0.1－45 keV) perpendicular and parallel temperature for all available events. Prior to zero epoch, proton perpendicular and parallel temperature are higher from the afternoon to midnight sector (12－24 LT). Following zero epoch, the temperature increases sharply, predominantly on the afternoon and night side with moderate enhancements at all local time. After an hour of the shock front arrival, both perpendicular and parallel temperature decrease significantly in the noon sector. It can be seen from Figures 7 and 8 that, following the shock front arrival, the proton population become hot and dense with a peak number density of 1.2 cm^{-3} compared to the typical number density of 0.7 cm^{-3}.

3.3 Density and temperature of electron response at the geosynchronous orbit

Figure 9 shows the results of superposed epoch analysis for hot electron (0.03－45 keV) number density for all available events. Prior to the zero epoch, the electron number density is low, especially on the day side. Following the zero epoch, the electron density shows a dramatic

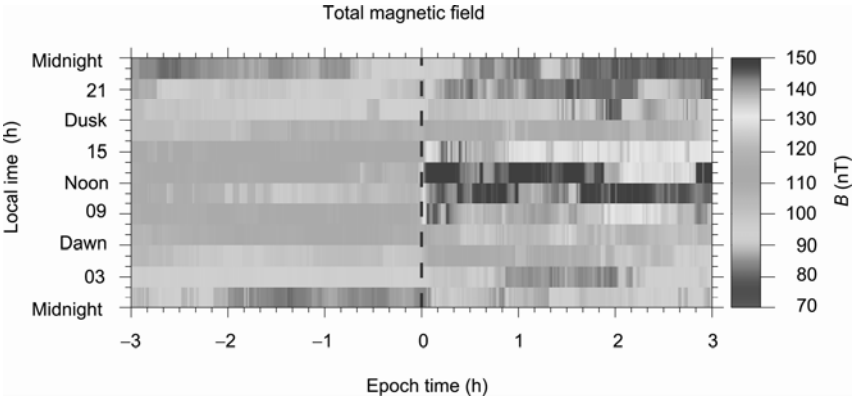

Figure 5 The UT-LT variation of the magnetic field magnitude for all available shock events at the geosynchronous orbit. The dashed line marks the shock arrival at the geosynchronous orbit.

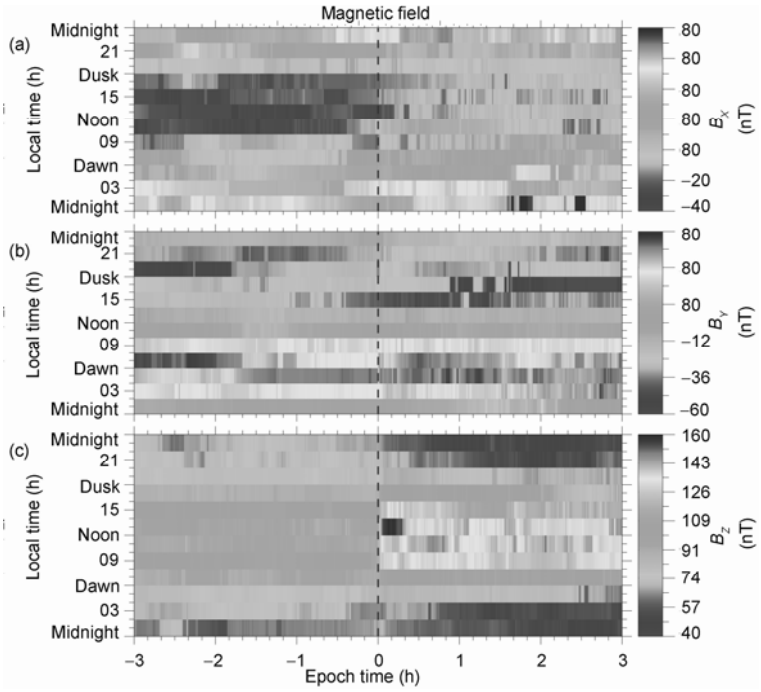

Figure 6 The UT-LT variation of the magnetic field in GSM for all available events at the geosynchronous orbit. (a) GSM B_X component; (b) GSM B_Y component; (c) GSM B_Z component. The dashed line marks the shock arrival at the geosynchronous orbit.

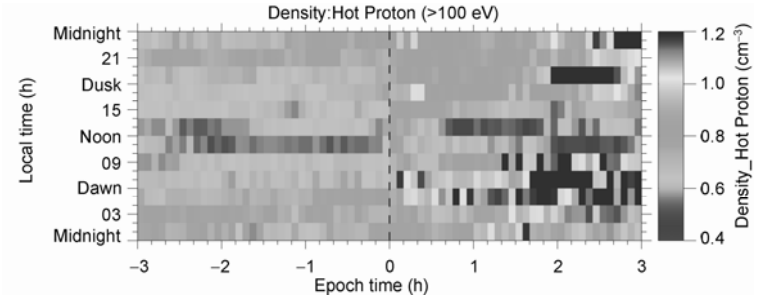

Figure 7 The UT-LT variation of the hot proton (0.1—45 keV) number density for all available events at the geosynchronous orbit. The dashed line marks the shock arrival at the geosynchronous orbit.

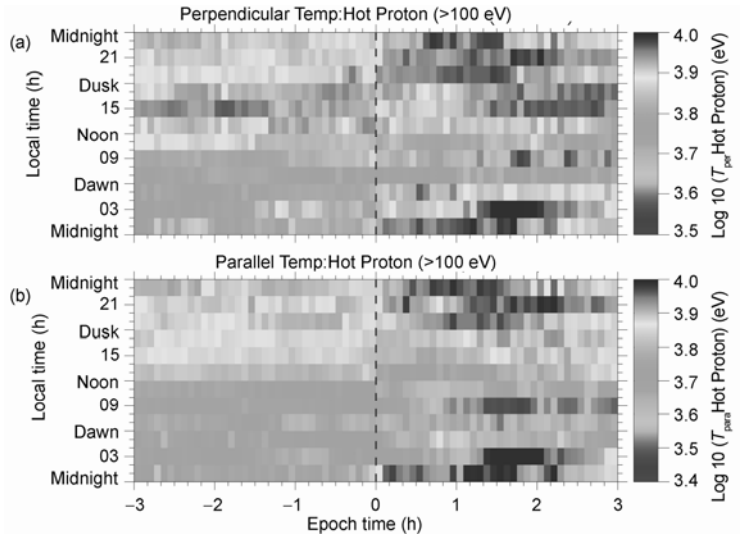

Figure 8 The UT-LT variation of the hot proton (HP) (0.1—45 keV) temperature for all available events at the geosynchronous orbit. (a) HP perpendicular temperature; (b) HP parallel temperature. The dashed line marks the shock arrival at the geosynchronous orbit.

increase, predominantly on the night side with the peak number density of 2.0 cm^{-3}.

Figure 10 shows the results of superposed epoch analysis for hot electron (0.03—45 keV) temperature for all available events. Prior to the zero epoch, the electron perpendicular and parallel temperatures are higher on post-midnight sector (24—6 LT). Following the zero epoch, the perpendicular and the parallel temperatures increase on the night side while decrease on the dayside. It can be seen from Figures 9 and 10 that, following the shock front arrival, the electron population becomes hot and dense.

3.4 The calculated O^+ and H^+ density and the O^+/H^+ density ratio

In the paper, we used the method from Denton et al.[14] to calculate the O^+ and H^+ density and O^+/H^+ density ratio at the geosynchronous orbit. Since the MPA instrument cannot directly distinguish ion composition, the ion population is assumed to be entirely composed of H^+. However, under the following conditions the MPA measurements may be used to estimate the concentration of O^+: (1) the hot plasma sheet populations measured by MPA (0.03 to 45 keV for the electrons and 100 eV to 45 keV for the ions) are much denser than any lower-energy populations present and (2) the contribution of higher-energy particles (>45 keV) to the density of either species is negligible[14]. Having considered the above assumptions, we choose the data selection criterion to be $1< N_{HE} / N_{HP} <4$, this criterion makes sure that the H^+ and O^+ density is larger than zero.

The hot electrons density measured by MPA is the sum of electrons from all ionized atoms. Thus during periods when O^+ is present (and neglecting the contribution of other ions) then, from charge neutrality, the density of the hot electrons, N_{HE}, is given by

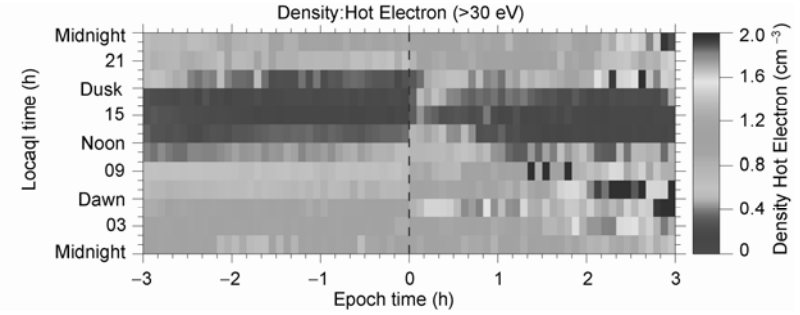

Figure 9 The UT-LT variation of the hot electron (0.03—45 keV) number density for all available events at the geosynchronous orbit. The dashed line marks the shock arrival at the geosynchronous orbit.

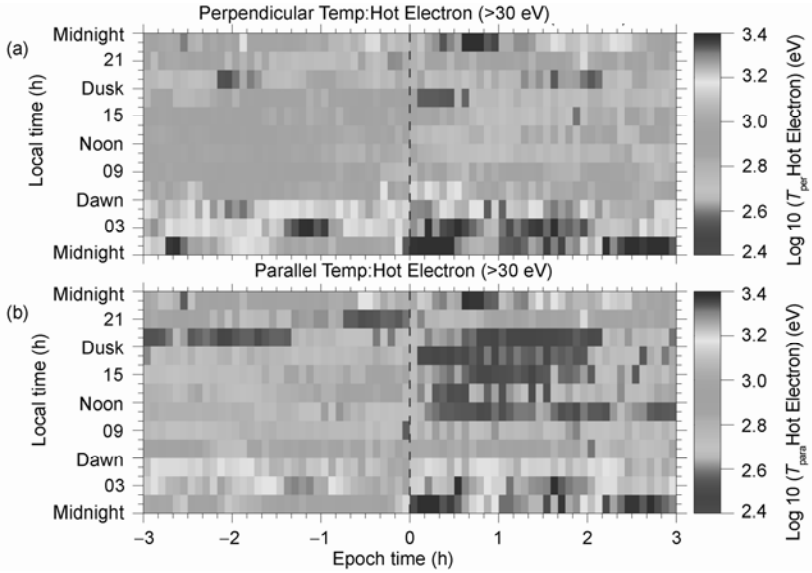

Figure 10 The UT-LT variation of the hot electron (HE) (0.03—45 keV) temperature for all available events at the geosynchronous orbit. (a) HE perpendicular temperature; (b) HE parallel temperature. The dashed line marks the shock arrival at the geosynchronous orbit.

$$N_{\mathrm{HE}} = N_{\mathrm{H^+}} + N_{\mathrm{O^+}}, \quad (1)$$

where $N_{\mathrm{H+}}$ is the H^+ density and $N_{\mathrm{O+}}$ is O^+ density.

The MPA instrument is an E/q analyzer and for normal operations the measured population is assumed to consist entirely of protons. From calculation of the velocity distribution function[30], the contribution to the total ion density of an ion species of mass m_i is given by

$$\sqrt{(m_p / m_i)}, \quad (2)$$

where m_p is the proton mass. Thus assuming that the total number of electrons and protons is equal, the nominal hot proton density, N_{HP}, is given by

$$N_{\mathrm{HP}} = N_{\mathrm{H^+}} + N_{\mathrm{O^+}} / 4. \quad (3)$$

Equations (1) and (3) can be rearranged and solved for the hydrogen density and the oxygen density so we get

$$N_{\mathrm{O^+}} = 4/3(N_{\mathrm{HE}} - N_{\mathrm{HP}}) \quad (4)$$

and

$$N_{\mathrm{H^+}} = (4N_{\mathrm{HP}} - N_{\mathrm{HE}})/3. \quad (5)$$

According to eqs. (1)—(5), the O^+ and H^+ density and O^+/H^+ density ratio can be calculated with MPA data at the geosynchronous orbit.

Figure 11 show the results of superposed epoch analysis for the inferred O^+ and H^+ number density and the O^+/H^+ density ratio. Prior to the zero epoch, the inferred O^+ number density is low, especially on the day side. The inferred H^+ density has the typical number density of 0.7 cm^{-3}, except on the afternoon sector. The O^+/H^+ density ratio is higher on the night side, predominantly on the dusk sector. Following the zero epoch, the inferred O^+ density increases at all local time. One hour after the zero epoch, the inferred O^+ density reaches the maximum value of 1.2 cm^{-3} on the dusk side. The inferred H^+ density increases rapidly on the night side after half an hour of the shock front arrival. The O^+/H^+ density ratio increases at all local time, especially on the dusk sector. Form figure 11, we know that the O^+ density shows the clear dawn-dusk asymmetry after the shock front arrival at the geosynchronous orbit. Sharp et al.[31] used the statistical analysis showing significant

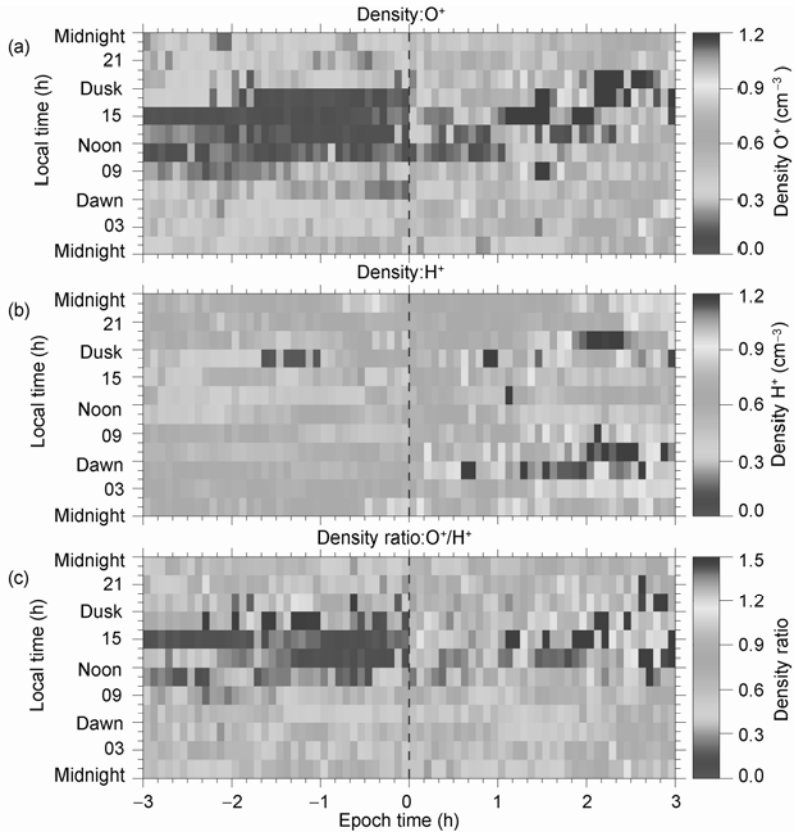

Figure 11 The UT-LT variation of the inferred O^+ and H^+ number density at the geosynchronous orbit. (a)The inferred O^+ number density; (b) the inferred O^+ and H^+ number density; (c) the O^+/H^+ density ratio. The dashed line marks the shock arrival at the geosynchronous orbit.

dawn-dusk asymmetries of low energy O^+ beams (energy typically 5 keV) in the near-earth plasma sheet with a strong performance in the dusk side of the plasma sheet. A strong dawn-dusk asymmetry in the occurrence frequency of auroral ion acceleration events had been pointed out by Ghielmetti et al.[32], with the highest probability on the dusk side. The statistical survey of oxygen bursts performed by Zong[33] has shown the dawn-dusk asymmetry in the distant tail could represent a simple expansion of an asymmetry already existing in the auroral oxygen extraction processes. Our results show that the interplanetary shock could induce the O^+ dawn-dusk asymmetry. However, it is necessary to take account of the valid region of the assumptions used in the calculation method. Denton et al.[14] pointed out that in the dusk sector, since electrons do not have access to the inner magnetosphere, the assumptions may be violated and the method may be less applicable. So, further studies with other measurements are needed to validate our results.

3.5 The temperature anisotropy of proton and electron

As already shown in the introduction part, the electromagnetic ion cyclotron (EMIC) wave and whistler wave may probably be stimulated by the proton and electron temperature anisotropy. So it is interesting to analyze the proton and electron temperature anisotropy and the EMIC wave and whistler wave frequency from the MPA data.

Here, we calculate the cutoff frequency of parallel propagating non-relativistic EMIC mode wave instability according to Horne and Thorne[17] as below:

$$\omega = \Omega_i A_i / (1 + A_i), \tag{6}$$

where $A_i = T_{\perp i} / T_{\|i} - 1$ is the proton temperature anisotropy, Ω_i is the proton gyrofrequency, and $T_{\perp i}$ and $T_{\|i}$ are the proton perpendicular and parallel temperature with regard to the magnetic field direction respectively.

We calculate the cutoff frequency of parallel propagating non-relativistic whistler mode wave instability according to Treumann and Baumjohann[34] as below:

$$\omega = \Omega_e A_e / (1 + A_e). \tag{7}$$

where $A_e = T_{\perp e} / T_{\|e} - 1$ is the electron temperature anisotropy, Ω_e is the electron gyrofrequency, and $T_{\perp e}$ and $T_{\|e}$ are the electron perpendicular and parallel temperature with regard to the magnetic field direction respectively.

Figure 12 shows the results of superposed epoch analysis for hot proton (0.1—45 keV) temperature anisotropy and the EMIC wave intensity for all available events. Prior to the zero epoch, the proton temperature anisotropy and the EMIC wave are higher on the day side. Following the zero epoch, the proton temperature anisotropy peak locates in the noon sector, and decreases towards dawn and dusk side. The EMIC wave intense on the day side (8—16 LT) with a frequency value of 0.8 Hz, and the wave intensity decreases towards the dawn and dusk side, the minimum value can be found on the night side. The electromagnetic ion cyclotron (EMIC) wave may probably be stimulated by the proton temperature anisotropy. The variation of the EMIC wave intensity is basically in consistent with those of magnetic field magnitude and proton temperature anisotropy, which is apparent according to the above formula.

Figure 13 shows the results of superposed epoch analysis for hot electron (0.03—45 keV) temperature anisotropy and the whistler wave for all available events. Prior to the zero epoch, the electron temperature anisotropy and the electron whistler wave are higher on the day side. Following the zero epoch, it's clear that the temperature anisotropy has almost no change on the day side while decreases dramatically on the night side. The electron whistler wave locates on the day side (8—16 LT) with a value of 2 kHz. It decreases towards the dawn and dusk side, minimizes on the night side.

4 Summary

(1) The arrival of shock front at the day side magnetopause induces a sharp enhancement in the magnetic field and plasma density, temperature and temperature anisotropies (electron and ions).

(2) The magnetic field magnitude enhances remarkably on the day side with a peak value of 160 nT following the shock front arrival. B_X increased only on the day side (8—16 LT) and almost has no change on the night side before and after the shock front arrival. B_Y almost has no change before and after the shock front arrival. B_Z component increases on the day side with the maximum of 160 nT while decreases on the night side.

(3) Following the shock front arrival, the proton population becomes hot and dense with a peak number density of 1.2 cm^{-3} compared to the typical number density

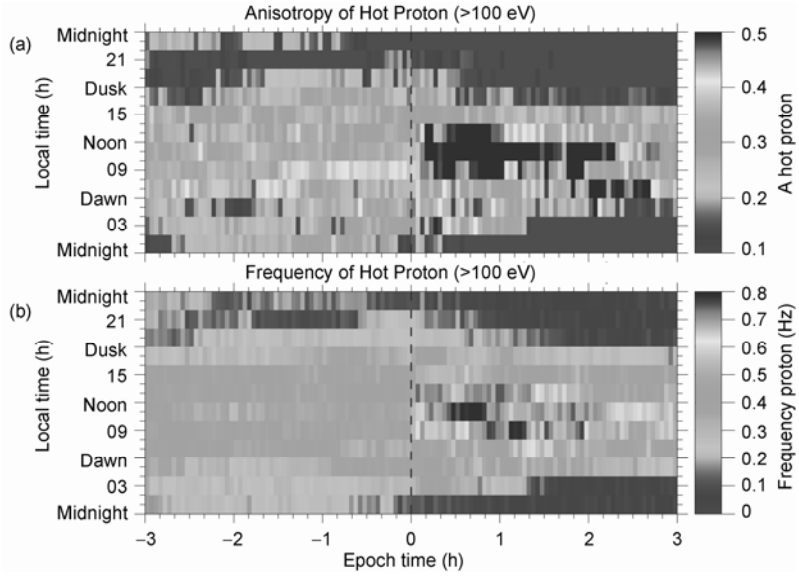

Figure 12 The UT-LT variation of the hot proton (HP) (0.1—45 keV) temperature anisotropy and the EMIC wave frequency for all available events at the geosynchronous orbit. (a) HP temperature anisotropy; (b) the EMIC wave frequency. The dashed line marks the shock arrival at the geosynchronous orbit.

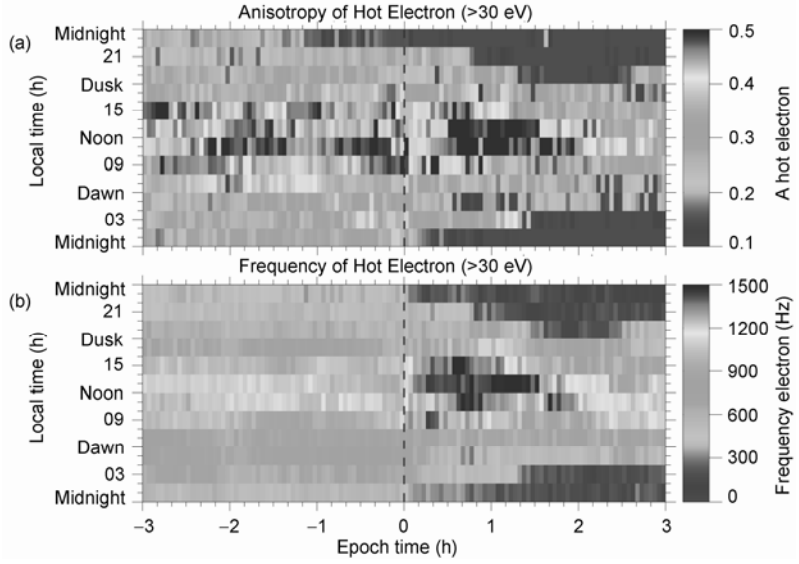

Figure 13 The UT-LT variation of the hot electron (HE) (0.03—45 keV) temperature anisotropy and the electron whistler wave frequency for all available events at the geosynchronous orbit. (a) HE temperature anisotropy; (b) the whistler wave frequency. The dashed line marks the shock arrival at the geosynchronous orbit.

of 0.7 cm^{-3}. The proton temperature increases sharply, predominantly on the afternoon and night side with moderate enhancements at all local time. The electron density shows a dramatic increase, predominantly on the night side with the peak number density of 2.0 cm^{-3}. One hour after shock front arrival, the inferred O^+ density reaches the maximum value of 1.2 cm^{-3} on the dusk side and shows the clear dawn-dusk asymmetry.

(4) The peak of the anisotropy of proton's temperature locates at the noon sector, and the anisotropy decreases towards the dawn and dusk side. The minimum of temperature anisotropy is on the night side.

(5) The electromagnetic ion cyclotron (EMIC) wave obtained from the temperature anisotropy intense on the day side (8—16 LT) with a frequency value of 0.8 Hz, and the wave intensity decreases towards the dawn and dusk side, the minimum value can be found on the night side.

(6) The electron whistler wave obtained from the temperature anisotropy locates on the day side (8—16 LT) with a value of 2 kHz. It is suggested that the electromagnetic ion cyclotron (EMIC) wave and whistler wave may probably be stimulated by the proton and electron temperature anisotropy respectively.

1 Rufenach C L, McPherron R L, Schaper J. The quit geomagnetic field at geosynchronous orbit and its dependence on solar wind dynamic pressure. J Geophys Res, 1992, 97: 25—42
2 Wang C, Liu J B, Huang Z H, et al. Response of the magnetic field in the geosynchronous orbit to solar wind dynamic pressure pulses. J Geophys Res, 2007, 112, A12210, doi:10.1029/2007JA012664
3 Patel V L, Coleman P J. Sudden impulses in the magnetosphere observed at synchronous orbit. J Geophys Res 1970, 75: 7255—7260
4 Lee D Y, Lyons L R. Geosynchronous magnetic field response to solar wind dynamic pressure pulse. J Geophys Res, 2004, 109, A04201, doi: 10.1029/2003JA010076
5 Borodkova N L, Zastenker G N, Riazantseva M, et al. Large and sharp solar wind dynamic pressure variations as a source of geomagnetic field disturbances at the geosynchronous orbit. Planet Space Sci, 2005, 53: 25—32
6 Lee D Y, Lyons L R, Reeves G D. Comparison of geosynchronous energetic particle flux responses to solar wind dynamic pressure enhancements and substorms. J Geophys Res, 2005, 110, A09213, doi: 10.1029/2005JA011091
7 Villante U, Piersanti M. An analysis of sudden impulses at geosynchronous orbit. J Geophys Res, 2008, 113, A08213, doi:10.1029/2008JA013028
8 Wang C, Liu J B, Li H, et al. Geospace magnetic field responses to interplanetary shocks. J Geophys Res, 2009, 114, A05211, doi:10.1029/2008JA013794
9 Borovsky E B, Thomsen M F, Elphic R C, et al. The transport of plasma sheet material from the distant tail to geosynchronous orbit. J Geophys Res, 1998, 103: 20297—20331
10 Elphic R C, Weiss L A, Thomsen M F, et al. Evolution of plasmaspheric ions at geosynchronous orbit during times of high geomagnetic activity. Geo Res Letters, 1996, 23: 2189—2192
11 Birn J, Thomsen M F, Borovsky J E, et al. Characteristic plasma properties during dispersionless substorm injections at geosynchronous orbit. J Geophys Res, 1997, 102: 2309—2324
12 Dandouras I, Henri R, Cao J B, et al. Magnetosphere response to the 2005 and 2006 extreme solar events as observed by the Cluster and Double Star spacecraft. Adv Space Res, 2008, 43: 618—623
13 Borovsky J E, Denton M H. Relativistic-electron dropouts and recovery: A superposed epoch study of the magnetosphere and the solar wind. J Geophys Res, 2009, 114, A02201, doi:10.1029/2008JA013128
14 Denton M H, Thomsen M F, Korth H, et al. Bulk plasma properties at geosynchronous orbit. J Geophys Res, 2005, 110, A07223, doi:10.1029/2004JA010861
15 Denton M H, Borovsky J E. Superposed epoch analysis of high-speed-stream effects at geosynchronous orbit: Hot plasma, cold plasma, and the solar wind. J Geophys Res, 2008, 113, A07216, doi:10.1029/2007JA012998
16 Kennel C F, Petschek H E. Limit on stably trapped particle fluxes. J Geophys Res, 1966, 71: 1—28
17 Horne R B, Thorne R M. On the preferred source location for the convective amplification of ion cyclotron waves, J Geophys Res, 1993, 98: 9233—9247
18 Cornwall J M, Coroniti F V, Thorne R M. Turbulent loss of ring current protons. J Geophys Res, 1970, 75: 4699—4709
19 Thorne R M, Horne R B. The contribution of ioncyclotron waves to electron heating and SAR-arc excitation near the storm-time plasmapause. Geophys Res Left, 1992, 19: 417—420
20 Cornwall J M, Coroniti F V, Thorne R M. Unified theory of SAR arc formation at the plasmapause. J Geophys Res, 1971, 76: 4428—4445
21 Bossen M, McPherron R L, Russel C T. A statistical study of Pc I magnetic pulsations at synchronous orbit. J Geophys Res, 1976, 81: 6083—6091
22 Xiao F L. Modelling energetic particles by a relativistic kappa loss cone distribution function in plasmas. Plasma Phys. Controlled Fusion, 2006, 48: 203—213
23 Xiao F L, Zhou Q H, He H Y, et al. Energetic electron distributions fitted with a relativistic kappa-type function at geosynchronous orbit. J Geophys Res, 2008，113，A05203, doi:10.1029/2007JA012903
24 Xiao, F L, Zhou Q H, Zheng H N, et al. Whistler instability threshold condition of energetic electrons by kappa distribution in space plasmas. J Geophys Res, 2006, 111, A08208, doi: 10.1029/2006JA011612
25 Xiao F L, Zhou Q H, He H Y, et al. Instability of whistler-mode waves by a relativistic kappa-loss-cone distribution inspace plasmas. Plasma Phys Controlled Fusion, 2006, 48, 1437—1445
26 Xiao F L, Zhou Q H, He H Y, et al. Electromagnetic ion cyclotron waves instability threshold condition of suprathermal protons by kappa distribution. J Geophys Res, 2007, 112, A07219, doi: 10.1029/2006JA012050
27 Singer H J, Matheson L, Grubb R, et al. Monitoring space weather with the GOES magnetometers. SPIE Proc, 1996, 2812: 299—308
28 Bame S J, McComas D J, Thomsen M F, et al. Rev Sci Instrum, 1993, 64: 1026—1033
29 McComas D J, Bame S J, Barraclough B L, et al. Magnetospheric plasma analyzer: Initial three-spacecraft observations from geosynchronous orbit. J Geophys Res, 1993, 98(A8): 13453—13465
30 Thomsen M F, Noveroske E, Borovsky J E, et al. Calculation of moments from measurements by the Los Alamos magnetospheric plasma analyzer. LA Rep LA-13566-MS, Los Alamos Natl Lab, Los Alamos, N M, 1999
31 Ghielmetti A G, Johnson R G, Sharp R D, et al. The latitudinal, diurnal, and altitudinal distributions of upward flowing energetic ions of ionospheric origin. Geophys Res Lett, 1978, 5: 59—62
32 Sharp R D, Carr D L, Peterson W K, et al. Ion streams in the magnetotail. J Geophys Res, 1981, 86: 4639—4648
33 Zong Q G. Energetic Oxygen Ions in Geospace Observed by Geotail Spacecraft. PhD dissertation. Brunswick: The Technical University Carolo-Wilhelmina, 1998. 118—123
34 Treumann R A, Baumjohann W. Advanced Space Plasma Physics. London: Imperial college, 1997:108—111